The American Journal of Pathology, Vol. 175, No. 5, November 2009

DOI: 10.2353/ajpath.2009.080792

Cardiovascular, Pulmonary and Renal Pathology

Effects of Increased Renal Tubular Vascular Endothelial Growth Factor (VEGF) on Fibrosis, Cyst Formation, and Glomerular Disease

Samy Hakroush,* Marcus J. Moeller,† Franziska Theilig,‡ Brigitte Kaissling,§ Tjeerd P. Sijmonsma,¶ Manfred Jugold,‖ Ann L. Akeson,** Milena Traykova-Brauch,¶ Hiltraud Hosser,* Brunhilde Hähnel,* Hermann-Josef Gröne,¶ Robert Koesters,†† and Wilhelm Kriz*

From the Centrum für Biomedizin und Medizintechnik Mannheim, Anatomy and Developmental Biology, Medical Faculty Mannheim, University of Heidelberg, Mannheim, Germany; the Division of Nephrology,† Rheinisch-Westfaelische Technische Hochschule, Aachen, Germany; the Department of Anatomy,‡ Charité, Berlin, Germany; the Department of Anatomy,§ University of Zürich, Zürich, Switzerland; the Department of Cellular and Molecular Pathology¶ and the Division of Medical Physics in Radiology,‖ German Cancer Research Center, Heidelberg, Germany; the Division of Pulmonary Biology,** Cincinnati Children's Hospital Research Foundation, Cincinnati, Ohio; and the Institute of Human Genetics,†† University of Heidelberg, Heidelberg, Germany*

The role of vascular endothelial growth factor (VEGF) in renal fibrosis, tubular cyst formation, and glomerular diseases is incompletely understood. We studied a new conditional transgenic mouse system [Pax8-rtTA/(tetO)$_7$VEGF], which allows increased tubular VEGF production in adult mice. The following pathology was observed. The interstitial changes consisted of a ubiquitous proliferation of peritubular capillaries and fibroblasts, followed by deposition of matrix leading to a unique kind of fibrosis, ie, healthy tubules amid a capillary-rich dense fibrotic tissue. In tubular segments with high expression of VEGF, cysts developed that were surrounded by a dense network of peritubular capillaries. The glomerular effects consisted of a proliferative enlargement of glomerular capillaries, followed by mesangial proliferation. This resulted in enlarged glomeruli with loss of the characteristic lobular structure. Capillaries became randomly embedded into mesangial nodules, losing their filtration surface. Serum VEGF levels were increased, whereas endogenous VEGF production by podocytes was down-regulated. Taken together, this study shows that systemic VEGF interferes with the intraglomerular cross-talk between podocytes and the endocapillary compartment. It suppresses VEGF secretion by podocytes but cannot compensate for the deficit. VEGF from podocytes induces a directional effect, attracting the capillaries to the lobular surface, a relevant mechanism to optimize filtration surface. Systemic VEGF lacks this effect, leading to severe deterioration in glomerular architecture, similar to that seen in diabetic nephropathy. ***(Am J Pathol 2009, 175:1883–1895; DOI: 10.2353/ajpath.2009.080792)***

Vascular endothelial growth factor (VEGF or VEGF-A) is a member of a family of heparin-binding growth factors that includes placental growth factor, VEGF-B, VEGF-C, VEGF-D (c-Fos-induced growth factor), and also the viral VEGF-E(s) of the parapoxvirus Orf. Alternative splicing of the *VEGF-A* gene leads to six different splice variants containing 121 (120 in mouse), 145, 165 (164 in mouse), 183, 189, and 206 amino acids (VEGF-A$_{121(120)\text{-}206}$). As homodimeric glycoproteins, VEGFs bind to two receptors: VEGFR2 (KDR/Flk-1) and VEGFR1 (Flt-1). A soluble variant of VEGFR1 is able to neutralize the effects of VEGF by binding VEGF within the circulation (reviewed by Ref. 1).

Supported by German Research Foundation Deutsche Forschungsgemeinschaft grant FOR 406 (to W.K. and R.K.) and grant FOR 667 (to F.T.) and grant SFB/TRR 57 TP17 (to M.J.M.) and grants by Prof. Dr. Karl und Gerhard Schiller-Stiftung (to W.K.) and the START-Program of the Faculty of Medicine, RWTH-Aachen (to M.J.M.).

S.H., M.J.M., R.K., and W.K. contributed equally to this work.

Accepted for publication July 24, 2009.

Supplemental material for this article can be found on *http://ajp.amjpathol.org*.

Address reprint requests to Wilhelm Kriz, M.D., Centrum für Biomedizin und Medizintechnik Mannheim, Medizinische Fakultät Mannheim der Universität Heidelberg, Anatomie und Entwicklungsbiologie, Ludolf-Krehl-Str. 13-17, Tridomus C, Ebene 6, 68167 Mannheim, Germany. E-mail: wilhelm.kriz@urz.uni-heidelberg.de.

VEGF-A is essential in mammalian vascular development by virtue of stimulating endothelial cell proliferation and differentiation. With respect to the kidney, VEGF is the primary mediator starting and directing glomerular development. In the adult, VEGF plays a central role in the intraglomerular regulatory network, accounting for the maintenance and repair of the glomerular tuft (reviewed by Ref. 2). VEGF is highly expressed in podocytes.[3] Even slight changes in the dose of VEGF cause dramatic aberrations in glomerular tuft structure.[4] In addition to podocytes, distal tubules, collecting ducts, and, to a lower degree, proximal tubules produce VEGF (reviewed by Ref. 5).

Currently, there is great interest in the pathogenetic role of VEGF in renal fibrosis, cystic tubular, and glomerular diseases, including diabetic nephropathy.[6–8] However, details are incompletely understood. We took advantage of a recently developed transgenic mouse model (Pax8-rtTA; Ref. 9) that allowed conditional overexpression of VEGF in the entire renal tubular system. Three major observations were made: 1) within the tubules themselves, VEGF stimulated cyst formation in a dose-dependent manner; 2) within the interstitium, VEGF stimulated the proliferation of peritubular capillaries and interstitial fibroblasts, followed by matrix deposition without damaging the tubules; and 3) within the glomerulus, increased serum VEGF decreased the production of VEGF by podocytes, thereby interfering with the intraglomerular cross-talk between podocytes and the endocapillary compartment. This led to glomerular injuries similar to lesion seen in diabetic glomerulopathy in humans.

Materials and Methods

Transgenic Animals and General Procedures

The experimental design of this study was approved by the local authorities according to the German law for protection of animals.

A conditional transgenic system was used to target VEGF (VEGF-A or $VEGF_{164}$) expression to the renal tubular system of adult mice. Two transgenic mouse lines were used: 1) Pax8-rtTA mice, which express the reverse tetracycline-dependent transactivator (rtTA) under control of the Pax8 promoter (specific for the entire tubular system of the kidney with a low expression in periportal hepatocytes);[9] and 2) $(tetO)_7$VEGF mice, which express a mouse transgene, coding for the isoform $VEGF_{164}$ of VEGF-A, under the control of tetracycline response elements [$(tetO)_7$].[10] Heterozygous Pax8-rtTA mice were crossbred with homozygous $(tetO)_7$-VEGF mice. Bitransgenic Pax8-rtTA/$(tetO)_7$-VEGF and single transgene control $(tetO)_7$-VEGF mice were obtained. VEGF was induced in renal tubules of bitransgenic 5-week-old mice by giving drinking water containing doxycycline (DOX; 1 mg/ml and 5% sucrose) and were fed a standard mouse chow (Sniff; Spezialdiäten, Germany). Single transgenic $(tetO)_7$-VEGF mice exposed to DOX were used as controls. All mice were genotyped by PCR analysis of tail DNA for Pax8-rtTA and $(tetO)_7$-VEGF transgenes.

The primers used were Pax8-rtTA: ST1, 5′-CCATGTCTAGACTGGACAAGA-3′; ST2, 5′-CTCCAGGCCACATATGATTAG-3′; and $(tetO)_7$VEGF, 5′-GTGCACTGGACCCTGGCTTTACTG-3′, 5′-ATGTGCTGGCTTTGGTGAGGTTT-3′.

Experimental Design

Three groups of mice (transgenics and controls) each consisting of seven animals of mixed gender were examined after 1, 2, and 4 weeks of DOX administration. An additional two animals were examined after 8 and 14 weeks of DOX treatment. Furthermore, 10 transgenic and 9 control animals after 4 weeks of DOX were taken for the assessment of tissue mRNA. No gender differences were observed.

Two days before sacrifice, ~200 μl of blood was collected by retrobulbar punction from each animal under ether anesthesia. Serum was separated by centrifugation (10 minutes at 1500 rpm); creatinine and urea were measured by an automatic analyzing system (Vitros 250 Chemistry System; Johnson & Johnson, Global Medical Instrumentation, Ramsey, MN), and VEGF levels were determined using a commercial ELISA (R&D Systems). To determine urinary protein excretion, the animals were placed in metabolic cages for 24 hours, and urine was collected and analyzed using the same system as mentioned above.

Animal Perfusion and Structural Studies

The mice were fixed by total body perfusion as described previously[11]. Briefly, under Nembutal anesthesia (50 mg/kg body weight, i.p.), after laparotomy a cannula was retrogradely inserted into the abdominal aorta below the exit of the renal arteries. Without prior flushing, the animals were directly perfused with 3% paraformaldehyde-PBS-fixative at a pressure of 220 mmHg for 3 minutes. Kidneys were removed, weighed, and cut into 1- to 2-mm-thick slices and postfixed in 3% glutaraldehyde-PBS overnight; thereafter, the slices were washed, and small blocks (2 × 3 mm) of cortex were cut, postfixed in OsO_4 (1% for 2 hours), and subsequently dehydrated and embedded into Epon by standard procedures. Semithin (1 μm thick) sections of each animal and, in addition, series of semithin sections of selected blocks as well as ultrathin sections of selected areas were cut on a ultracut microtome (Leica, Nussloch, Germany) using a diamond knife. Semithin sections were stained with methelyne blue[12] and examined with light microscopy; ultrathin sections were stained with uranyl acetate and lead citrate and studied with transmission electron microscopy.

Morphometry

Morphometric analysis was performed with a semiautomatic image analysis system (VIDS IV; AiTectron, Düsseldorf, Germany). The tuft volume (VT) was estimated of seven transgenic animals and seven controls after 1, 2, and 4 weeks of DOX administration. Under direct visualization (magnification, ×20), the tuft areas (ATs) of 60

consecutive cross-sectional glomerular profiles per animal were measured on a digitizing tablet. VT was calculated from the mean tuft area, using the formula: $VT = (\beta/k)(AT)^{3/2}$, where $\beta = 1.38$ (shape coefficient for spherical particles) and $k = 1.1$ (size distribution coefficient for spheres).[13]

A semiquantitative estimate of podocyte density was assessed in 4-μm paraffin sections stained with antibodies against WT-1 of seven transgenic and five control animals after 2 and 4 weeks of DOX. WT-1-positive nuclei (podocytes) were counted in 30–40 glomerular profiles (fairly cut through the center of a glomerulus in meridian direction), and the density was calculated by relating the number of positive nuclei to the measured tuft area.

Interstitial expansion was determined in light micrographs of semithin sections of seven transgenic and seven control animals after 2 weeks of DOX. Per animal, two random areas of renal cortex (640 $\times$ 500 μm each) were analyzed using a transparent point raster (266 points; point distance, 33 μm); points overlying the interstitium were counted and a fractional area was calculated.

Cell proliferation was assessed with the Ki-67 antibody technique in 4-μm-thick paraffin sections of seven transgenic and seven control animals after 2 and 4 (only in glomeruli) weeks of DOX. Ki-67-positive cells in the interstitium were counted in 50 random areas of renal cortex (320 $\times$ 250 μm each), and a ratio per 1 mm^2 was calculated. Ki-67-positive glomerular cells were counted in 30 randomly selected glomeruli per animal.

In Situ *Hybridization*

The mRNA expression of VEGF, platelet-derived growth factor (PDGF)-B, and transforming growth factor (TGF)-β were investigated by *in situ* hybridization using digoxigenin-labeled riboprobes (Roche). Sense and antisense probes were generated by *in vitro* transcription of ~400 bp VEGF cDNA, ~700 bp PDGFB, and ~700 bp TGF-β cDNA of the coding region.

In situ hybridization was performed on 5-μm-thick paraffin sections according to an established protocol.[14] Signal was generated with 4-nitroblue tetrazolium chloride. For control, sense probes were applied in parallel with antisense probes.

Immunofluorescence Microscopy

Coronal slices comprising the cortex and the outer medulla were embedded into OCT compound (Tissue-Tek) and frozen in liquid isopentane cooled with liquid nitrogen. Four-micrometer-thick sections were cut in a cryostat (Microm, Walldorf, Germany) and stained, using the following antibodies: polyclonal rabbit anti-rat ecto-5-nucleotidase (5′NT) antibody, Le Hir[15], polyclonal rabbit anti-mouse α-smooth muscle actin (α-SMA) antibody (Abcam, Cambridge, UK); polyclonal rat anti-mouse major histocompatibility complex class II antibody, clone M5/114,15.2, and polyclonal rabbit anti-mouse proliferating cell nuclear antigen antibody (Santa Cruz Biotechnology, Heidelberg, Germany); and polyclonal goat anti-mouse platelet/endothelial cell adhesion molecule-1 (CD31) antibody (Santa Cruz Biotechnology). For double-staining procedures, antibodies were incubated consecutively.

Immunohistochemistry

Immunohistochemistry with the avidin-biotin technique was performed on 4-μm paraffin sections of paraformaldehyde-perfused tissue according to an established protocol[16].

The following antibodies were used: polyclonal goat anti-human VEGF antibody (1/140) (R&D Systems); polyclonal rabbit anti-rat type I collagen antibody (1/100) (Biotrend, Köln, Germany); polyclonal rabbit anti-human type IV collagen antibody (1/100) (Progen); polyclonal rabbit anti-human WT-1 antibody (1/100) (Santa Cruz Biotechnology); polyclonal rabbit anti-human Ki-67 antibody (1/50) (Dako); monoclonal rat anti-mouse Meca 32 antibody (1/100) (Santa Cruz Biotechnology); monoclonal rat anti-mouse ER-HR3 antibody (1/20) (Acris Antibodies, Hiddenhausen, Germany); and polyclonal rabbit anti-human PDGF-B antibody, LS-B1291 (Lifespan Bioscience). For all antibodies, negative controls were used in which the primary antibody was omitted. Specificity of VEGF antibody was controlled by blockade of the antibody using the respective recombinant $VEGF_{164}$ protein.

Western Blotting

Total kidney homogenate was produced using radioimmunoprecipitation assay buffer containing protease inhibitor mixture (Complete) and centrifuged to remove debris. Total protein concentration was measured using Pierce BCA Protein Assay reagent kit (Pierce, Rockford, IL). Fifty micrograms of protein was loaded onto 10% polyacrylamide gels. After SDS-PAGE and electrophoretic transfer of proteins to nitrocellulose membranes, equity in protein loading and blotting was verified by membrane staining using Ponceau red. Membranes were probed overnight with anti-VEGF and then exposed to horseradish peroxidase-conjugated anti-goat antibody (Dako). Immunoreactive band was detected on the basis of chemiluminescence, using an enhanced chemiluminescence kit (Amersham Biosciences, Freiburg, Germany) before exposure to X-ray films (Hyperfilm; Amersham Biosciences). For densitometric evaluation of the resulting bands, films were scanned and analyzed using BIO-PROFIL Bio-1D image software (Vilber Lourmat, Marue La Vallee, France).

Isolation of Glomeruli and Tubulointerstitial Tissue

Four control and four transgenic mice (after 4 weeks of DOX) were narcotized by i.p. injection of sodium pentobarbital (0.06 mg/g body weight). Kidneys were then perfused retrogradely through the abdominal aorta using 8×10^7 Dynabeads (M-450 Tosylactivated) diluted in 40 ml of HBSS containing 1 mg/ml collagenase A. Kidneys

Table 1. Clinical Data

	1 week DOX		2 weeks DOX		4 weeks DOX	
	TGM	CM	TGM	CM	TGM	CM
General data						
Body weight (g)	17.78 ± 0.672	18.47 ± 0.832	19.27 ± 0.693	20.73 ± 0.663	21.61 ± 1.617	22.81 ± 0.708
Serum						
Creatinine (μmol/L)	13.29 ± 0.969	13.43 ± 2.010	16.29 ± 1.584	15.43 ± 1.556	13.00 ± 2.400	15.00 ± 0.845
Urea (mmol/L)	13.29 ± 0.961	14.14 ± 1.990	10.60 ± 1.759	8.171 ± 0.651	11.31 ± 2.890	6.614 ± 0.506
Urine						
Protein (mg/24 hours)	2.730 ± 1.576	2.296 ± 1.131	0.208 ± 0.090	1.939 ± 1.000	4.999 ± 2.261	1.804 ± 0.691

Values are mean ± SEM; TGM and CM represents transgenic mice and control mice, respectively. $N = 7$. Student's *t*-test: no significant changes.

were removed, minced, and digested with HBSS containing 1 mg/ml collagenase A at 37°C for 30 minutes with gentle agitation. Glomeruli-containing Dynabeads were gathered by a magnetic particle concentrator, and quality was controlled by microscopical analysis. The remaining tubulointerstitial tissue was centrifuged for 15 minutes at 1000 × *g*, and resulting pellets were shock-frozen (compare Ref. 17). In addition, six transgenic and five control animals (after 4 weeks of DOX, perfusion, and handling as described above) were used to obtain total renal tissue, ie, without removal of a glomerular fraction.

RNA Isolation, Reverse Transcription, and Real-Time PCR

Total RNA was extracted from the glomerular, the tubulointerstitial tissue and the total kidney fraction using RNeasy Mini kit (Qiagen, Hilden, Germany). Genomic DNA was digested by DNase I (Invitrogen), and cDNA was synthesized by reverse transcription of 5 μg of total RNA (SuperScript First-Strand Synthesis System; Invitrogen). TaqMan Gene Expression Assays were used, and the product IDs are for VEGF-A Mm00437306_m1, TGF-β Mm03024053_m1, and PDGF B Mm01298578_m1. The experiment was performed according to the manual provided by Applied Biosystems (Foster City, CA). Amplification was performed using the real-time PCR TaqMan Fast 7500 (Applied Biosystems). Threshold cycle (C_t) values were set in the linear phase of exponential amplification. The difference (ΔC_t) between values obtained for VEGF, TGF-β, PDGF-B, and the housekeeping gene glyceraldehyde-3-phosphate dehydrogenase was calculated and the resulting values of $2^{\Delta\Delta Ct}$ were compared between controls and transgenics and expressed as fold increase. The values of the tubulointerstitial fraction and the total kidney fraction were considered as comparable.

Ultrasound Scan

Ultrasound scan (US) measurements were performed using the Vevo 770 microultrasound system (VisualSonics, Toronto, Ontario, Canada). The transducer transmits at a ..center frequency of 40 MHz with a focal length of 6 mm. Doppler frequency is 30 MHz. Three animals were examined before and after 4 weeks of DOX. For ultrasound examination, the mice were anesthetized by inhalation of a mixture of isofluorane (1.5%) and O_2 (98.5) and fixed on an examination table.

In the examination area the fur was removed carefully. The back of the mice were covered with ultrasound gel (Aquasonic 100; Fa. Parker; Fairfield, USA). Artificial embedding of air bubbles in the gel was avoided. An ultrasound transducer, fixed on a motor-driven unit above the animal, was moving perpendicularly to the beam axis, thereby acquiring consecutive images with a slice thickness of 100 μm. Regions of interest were drawn by hand around kidney borders on every fifth acquired ultrasound two-dimensional slice. Color pixel density of the cortex of the kidneys was evaluated in a smaller area close to the scanhead of the transducer to avoid artifacts due to signal loss in deeper tissue (compare with Ref. 18).

Statistical Analyses

Results are reported as mean ± SD Differences between the experimental and control animal in each group were tested with the unpaired *t*-test using Graphpad Prism 5.0.

Results

To further investigate the role of VEGF within the kidney, Pax8-rtTA mice[9] were used to overexpress murine $VEGF_{164}$ in renal tubular cells in a DOX-dependent manner. The effects were studied at various time points between 1 and 14 weeks after DOX administration.

None of the induced animals showed signs of distress; no significant differences in body weight and serum levels of urea and creatinine between controls and experimental animals were noticed. The animals did not develop any significant proteinuria (Table 1).

Overexpression of VEGF was verified by real-time-PCR, *in situ* hybridization, and immunohistochemistry (Figures 1A and 2, A and C) and Western blotting. VEGF expression was up-regulated in all tubular segments throughout the kidney. Western blot analysis displayed one specific single band at 25 kDa, which was controlled by antibody blockade experiments (Supplemental Figure S1, see *http://ajp.amjpathol.org*). Compared with the respective control mice, transgenic mice demonstrated a strong increase in VEGF expression levels (control 100.0 ± 13.7% and transgenic 753.4 ± 62.8%; $P <$

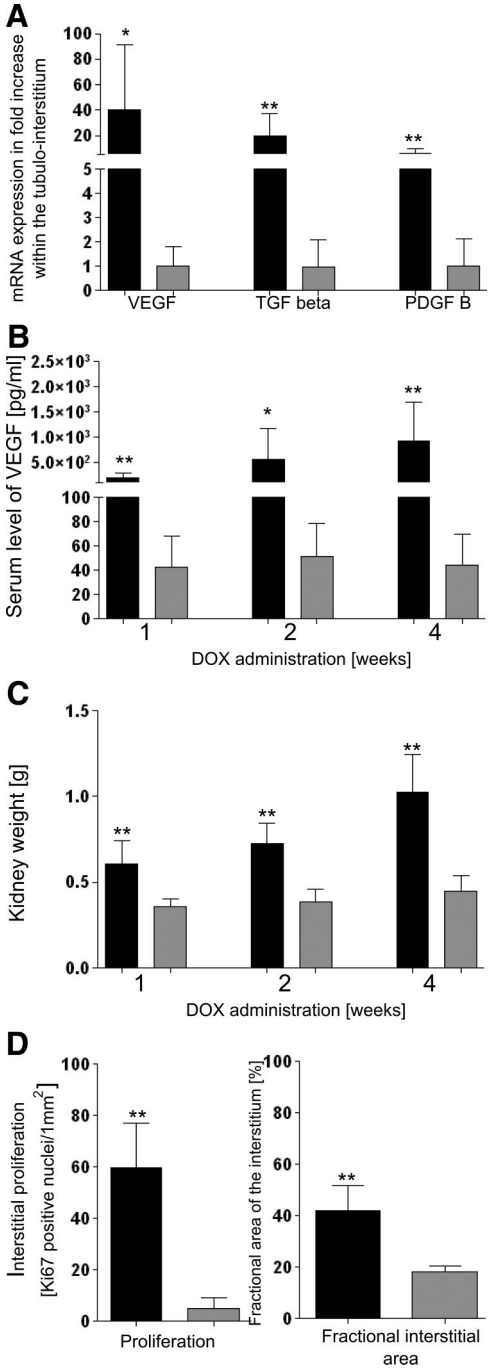

Figure 1. Values of experimental animals in black, controls in gray columns; shown are the means ± SD. **A:** mRNA expression within the tubulo-interstitium after 4 weeks of DOX; compared with controls, expression of VEGF, TGF-β, and PDGF-B is up-regulated. N (transgenics) = 10 (tubulo-interstial and total kidney samples were pooled), N (controls) = 9; *, $P < 0.05$; **, $P < 0.01$. **B:** Serum levels of VEGF. After 1, 2, and 4 weeks of DOX, transgenic animals exhibit increased serum levels of VEGF in comparison with control mice. $N = 7$; *, $P < 0.05$; **, $P < 0.01$. **C:** Kidney weight. After 1, 2, and 4 weeks of DOX, a dramatic increase in kidney weight is noticed in transgenic mice compared with controls. $N = 7$; **, $P < 0.01$. **D:** Interstitial cell proliferation and fractional interstitial area. After 2 weeks of DOX, transgenic animals show a strongly elevated number of Ki-67-positive cells within the peritubular interstitium (comprising all interstitial cells including endothelial cells) together with an enormous expansion of the peritubular interstitium. $N = 7$; **, $P < 0.01$.

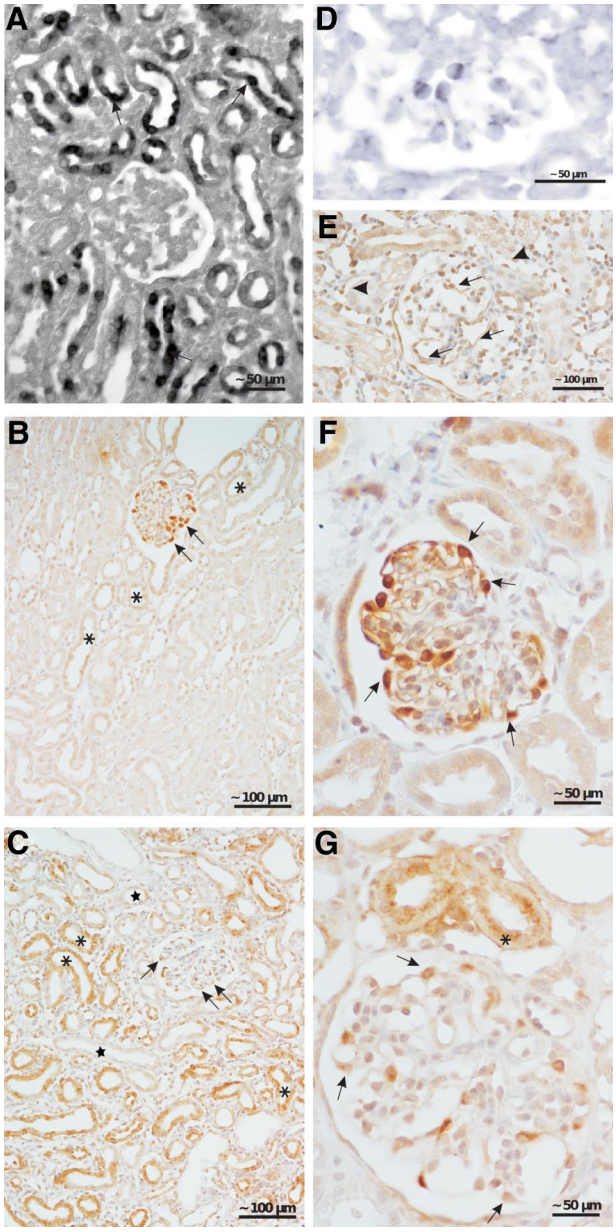

Figure 2. VEGF and PDGF-B. **A:** *In situ* hybridization of VEGF. In transgenic animals a heterogeneous tubular expression of VEGF mRNA (**arrows**) is encountered; no signal is seen with the sense probe (data not shown). **B**, **C**, **F**, and **G:** Immunohistochemistry of VEGF. **B** and **F:** In controls, a strong staining in podocytes (**arrows**) and a very weak staining in some tubules (**asterisks**) are seen. **C** and **G:** In transgenic animals, a strong but heterogenous staining is encountered; the majority of tubules shows a strong staining (**asterisk**); a couple of tubules (stars) do not show any reaction. Staining intensity in podocytes is decreased (**arrows**). **D:** *In situ* hybridization of PDGF-B. Note the expression in glomerular endothelial cells. In controls, no reaction was seen (data not shown). **E:** Immunohistochemistry reveals a strong expression PDGF-B in glomerular (**arrows**) and peritubular endothelial cells (**arrowheads**). Two weeks of DOX (**A**, **D**, and **E**); 4 weeks of DOX (**B** and **C**).

0.001). The expression was heterogeneous in the sense that a mosaic of positive and negative tubular cells was encountered. Since positive cells represented the majority, with respect to the entire kidney, the expression was very homogeneous and robust. The increased tubular production led to increased levels of VEGF within the serum (as detected by enzyme-linked immunosorbent

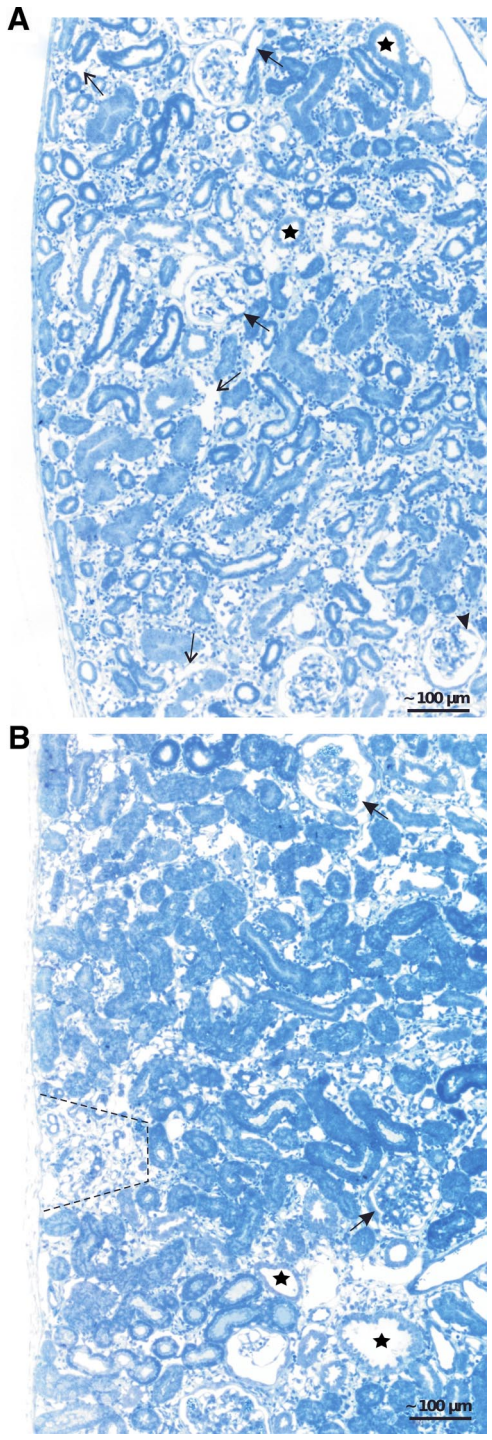

Figure 3. Renal cortex; overviews. **A:** After 2 weeks of DOX, ubiquitous expansion of the peritubular space with an increased density of interstitial cells and enlargement of capillaries (**thin arrows**). Tubules are heterogeneous in diameter; some of them (**stars**) show the beginning of cyst formation. Glomeruli show enlarged afferent arterioles (**arrows**), dilated capillaries (**arrowhead**), and focal centers of mesangial expansion. **B:** After 4 weeks, the expansion of the peritubular spaces is largely preserved; tubules in such areas look normal. In circumscribed areas (marked by a hatched line), tubules undergo atrophy/degeneration corresponding to the area of a nephron in which degeneration started from a glomerular damage. Individual tubular cysts (**stars**) are also encountered. Glomeruli show nodule formation (**arrows**).

assay; Figure 1B). As expected, the Pax8 promoter did not confer any activity on the glomerulus.

Prominent structural changes were found 1) in the peritubular interstitium, where a unique kind of fibrosis developed, 2) in renal tubules themselves, which frequently showed cyst formation, and 3) in glomeruli, which finally led to nephron degeneration and fibrosis.

Interstitial Changes

On inspection of the abdomen at the day of sacrifice the kidneys stood out by their increase in size (Figure 1C) and their intense red color. An increased blood content was also detected *in vivo* by ultrasound measurements (Supplemental Figure S2, see *http://ajp.amjpathol.org*).

In histological sections a ubiquitous and dramatic proliferation of peritubular capillaries and interstitial cells was seen leading to a massive expansion of the capillary and total peritubular space (Figures 1D, 3, A and B, and 4A). The increase of proliferating Ki-67-positive interstitial cells comprised all peritubular cells. Double immunolabeling with proliferating cell nuclear antigen and CD31 revealed proliferation of endothelial cells (Figure 4E). The increase in 5′NT and α-SMA-positive cells (Figure 5, A–C) indicated an accumulation of fibroblasts and myofibroblasts, also seen by transmission electron microscopy (Supplemental Figure S3, see *http://ajp.amjpathol.org*). In contrast, the density of major histocompatibility complex class II-positive (mostly dendritic cells) did not increase (Figure 5). Macrophages (specifically labeled with ER-HR3) were encountered only in later stages predominantly in areas of secondary fibrosis (see below). Real-time PCR and *in situ* hybridization revealed increased expression of PDGF-B and TGF-β within the tubulo-interstitium (Figures 1A and 4, F and G), ie, in cells of the interstitium, probably mostly endothelial cells supported by the anti-PDGF-B immunohistochemical stainings (Figure 2E).

The newly formed capillaries were closely apposed to the tubules and had unusually wide lumina resembling blood sinuses lined by densely arranged endothelial cells (Figure 4, A and B). In general, the endothelium was fenestrated; however, endothelial areas with nondiaphragmed fenestrae were frequently encountered (Figure 4, C and D).

The interstitial spaces proper between tubules and capillaries consisted of cells (see above) and abundant newly formed matrix that contained masses of collagen I and IV (Figure 6, B and C). Thus, a unique situation had developed: healthy tubules were embedded into a capillary-rich dense fibrotic tissue (Figure 6, A–C). Despite the ubiquitous appearance of myofibroblasts, up-regulation of α-SMA in tubular epithelia, considered to indicate epithelial-to-mesenchymal transformation,[19] was not observed. This indicated that no epithelial-to-mesenchymal transformation of tubular cells occurred in this model.

Tubular Effects

Changes in the tubules were generally seen beginning after 2 weeks of DOX administration and steadily increas-

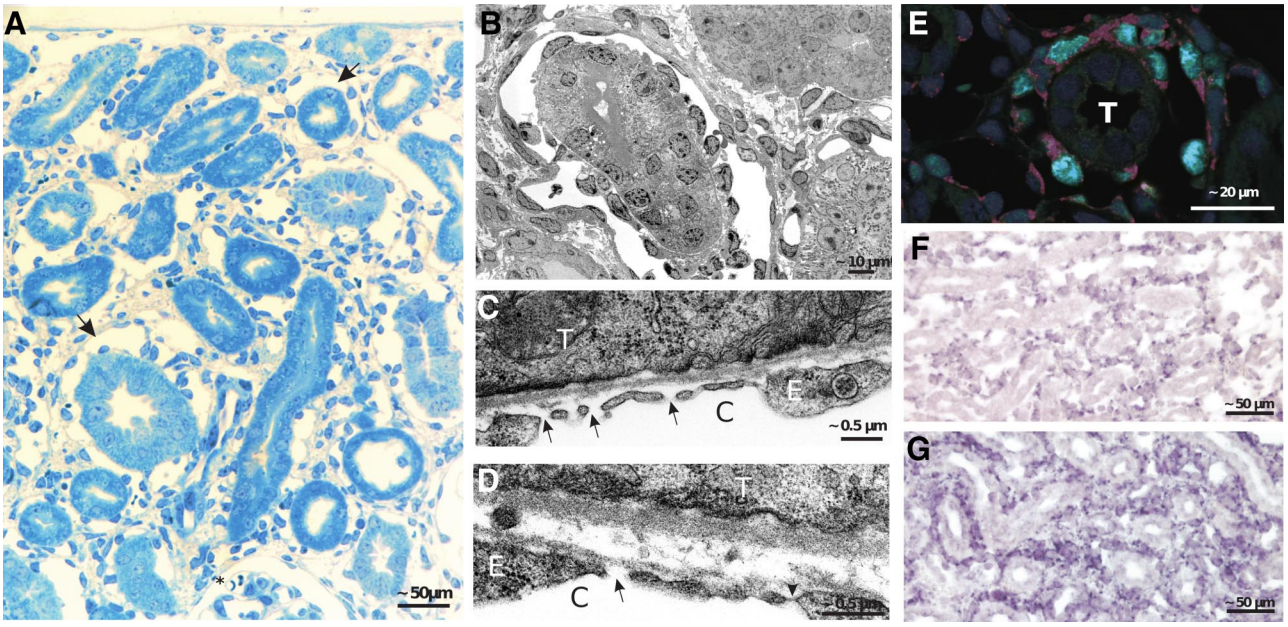

Figure 4. Peritubular interstitium and capillaries after 2 weeks of DOX. **A:** Within the expanded interstitium capillaries are enlarged at many sites to giant vascular channels completely surrounding a tubular profile (**arrows**). Note the abundance of interstitial cells and matrix; tubules are normal. **B:** Enlarged peritubular capillary completely surrounding a tubular profile; note the high density of endothelial cells. Frequently, areas equipped with a porous endothelium, ie, with undiaphragmed fenestrae are observed (**arrows** in **C** and **D**); the **arrowhead** in **D** points to a diaphragmed fenestra for comparison. C, capillary; E, endothelium; T, tubule. **E:** Immunofluorescence. Double-labeling against proliferating cell nuclear antigen (green) and CD31 (red) emphasizes the vivid proliferation of endothelial cells of an enlarged peritubular capillary; T, tubule. **F** and **G:** *In situ* hybridization reveals a prominent expression of PDGF-B **(F)** and TGF-β **(G)** in cells of the peritubular interstitium, mostly probably endothelial cells. In controls, no signals were observed; sense probes were negative (data not shown).

ing thereafter. Two types of direct tubular changes were encountered: shedding of cytoplasm and cyst development.

Conspicuously damaged tubules were noticed in animals at any of the analyzed time points (Supplemental Figure S4, see *http://ajp.amjpathol.org*). Large epithelial areas had shed major parts of their cytoplasm into the tubular lumen. Underneath, the cells survived as a thin layer of intact epithelium resting on the basement membrane. These changes did not appear to progress any further, probably because of recovery of the epithelium.

Cystic dilatation of segments was seen in proximal, distal, and collecting tubules (Figure 7A); many Ki-67-positive cells and mitoses indicated that cysts expanded by ongoing cell proliferation. Their frequency did not increase over time. In later stages, the cells dedifferentiated into a simple flat epithelium. VEGF expression in such tubular cysts was consistently high (Figure 7B). Cysts were surrounded by a capillary-rich fibrous tissue (Figure 7C).

In later stages, secondary tubular changes subsequent to glomerular damage were encountered, which are described below.

Glomerular Changes

The glomerular changes were ubiquitous and, in the first 2 weeks, of a uniform pattern. They consisted of prominent expansion of the glomerular vessels followed, generally with a delay of 1 week, by mesangial proliferation resulting in massively enlarged glomeruli (Figure 8, A and B). In addition, starting with 2 weeks in a small, albeit increasing, fraction of glomeruli, secondary changes developed that appeared to initiate the degenartion of the respective nephron (see below).

Thus, the initial changes specific to this model consisted of extensive proliferations of endothelial and mesangial cells. Relevant in this respect appear to be the increased serum levels of VEGF (Figure 1B) together with a decreased expression of VEGF in glomeruli shown at the mRNA level (Figure 8C). As shown by immunohistochemistry, VEGF expression was strongly down-regulated in podocytes (Figure 2, B, C, F, and G). Expression of PDGF-B was up-regulated at the mRNA level in isolated glomeruli (Figure 8C). PDGF-B was predominantly produced by endothelial cells as shown by *in situ* hybridization (Figure 2D) and by immunohistochemistry (Figure 2E).

The following describes the changes in detail: the sequence started with an overall enlargement of glomerular vessels, including the afferent and efferent arterioles (Figures 9 and 10). The capillary enlargement was associated with hyperplasia (ie, growth in width and length) and dilation with simplification of the tortuous capillary pattern. Thus, in sections through the tuft, fewer but much larger capillary profiles were encountered. Glomerular endothelial cells were increased in density and frequently found in unusual locations (Figures 9, A and B, and 10, A and D). Normally, endothelial cell bodies are located adjacent to the mesangium; here, they were seen at any position in the capillary even peripherally beneath podocyte cell bodies. Wide lumina and a considerable increase in endothelial cell density were also seen in glomerular arterioles, especially the intraglomerular segment of the efferent arteriole (Figure 9C).

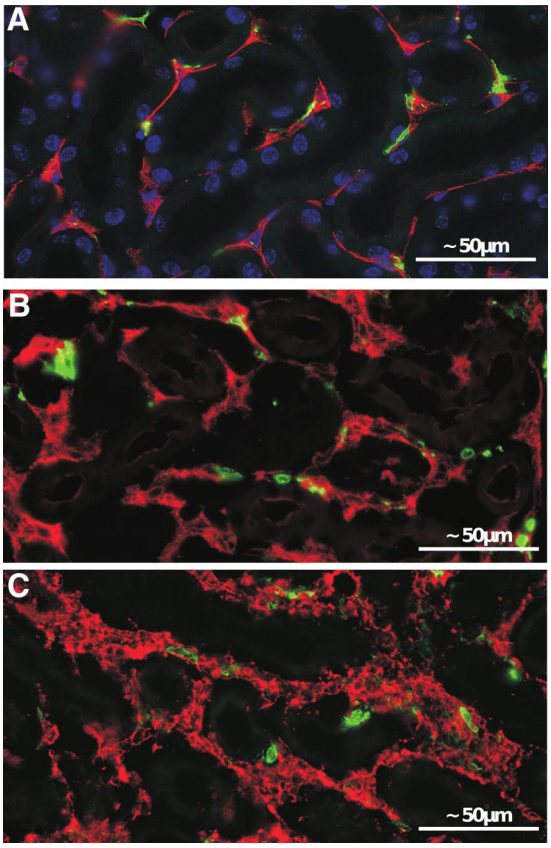

Figure 5. Expanded peritubular spaces after 2 weeks of DOX. **A–C:** Immunofluorescence. Staining against 5′NT (red in **A** and **B**) and α-SMA (red in **C**) and major histocompatibility complex class II (green). A pronounced increase of 5′NT-positive fibroblasts is seen in **B** compared with the control (**A**). A dramatic appearance of α-SMA-positive myofibroblasts is seen in **C**; in controls, no myofibroblasts are observed (data not shown). No differences in major histocompatibility complex class II-positive cells (green) are seen.

At this early stage, the mesangium was not particularly enlarged (Figures 9B and 10, A and D); small, clustered foci of cells and matrix, centrally associated with enlarged capillaries, were sometimes found. The changes in podocytes were moderate. Because of the enormous glomerular enlargement, the density of podocytes was drastically decreased (Figure 8D). Podocyte cell bodies appeared hypoplastic, but stereological assessments did not show any differences in cell body volume (data not shown). The primary processes were thinned out to cytoplasmatic sheets (Figure 10H); the interdigitating foot process pattern was unaltered apart from focal sites of effacement in later stages.

Beginning after 2 weeks, more frequently after 4 weeks and consistently after 8 or more weeks, mesangial proliferation dominated the picture (Figures 9C and 10, B and E). The increase in mesangial tissue was associated with a reorganization of the larger capillaries into smaller subunits; however, few large capillary profiles were preserved in most glomeruli.

These changes resulted in glomerular lobules with an abnormal architecture (Figures 9C and 10B). Most of the small capillaries no longer bulged into Bowman's space. Instead, they were progressively buried into the expanding mesangium, eventually losing their contact to the glomerular basement membrane (GBM) entirely so that they had no longer any free filtering surface (Figures 10, B and F). The mesangium in between the capillaries consisted of extensively branched cells and enormous amounts of matrix completely filling the intricate spaces between the capillaries, the GBM, and the mesangial cell processes. Amid such areas of mesangial expansion, capillary remnants were frequently encountered. They consisted of defective profiles with narrow lumina or just of wrinkled residues of the porous endothelium (Figures 10, C and G). Taken together, mesangial proliferation and capillary degeneration led to the development of nodular glomerular lobules that consisted of the expanded mesangium enclosing small capillaries with little or no filtering surface. These nodular structures were surrounded by a GBM that had largely lost any infoldings. Surprisingly, the podocytes had generally preserved their interdigitating foot process pattern.

The GBM itself did not show any conspicuous changes in appearance or in thickness. In late stages at sites of mesangial expansion, it became difficult to clearly discriminate in transmission electron microscopies the GBM from the mesangial matrix. Capillaries that were fully enclosed within the mesangium synthesized their own basement membrane.

On top of these model-specific changes, which affected all glomeruli, in a fraction of glomeruli "classic" injuries were focally encountered. They consisted of tuft adhesions to Bowman's capsule combined with proliferative capsular changes that encroached on the glomerulo-tubular junction. In the vicinity of such glomeruli, groups of atrophic/degenerating tubules were generally found (Figures 3 and 6D). Tracing in serial sections revealed that degenerating tubules were only encountered when associated with specifically injured glomeruli, ie, when the glomerular damage had encroached on the tubule alongside the urinary orifice. In such areas, macrophages were frequently encountered (Figure 6E), the abundance of capillaries disappeared, and a progressive fibrosis of the "classic type" developed (Figure 6F).

Discussion

VEGF plays an essential role in nephron development and in maintenance of kidney integrity in the adult.[2,4,20] It is continuously produced in podocytes and also to a lesser extent in tubules.[5] The Pax8 promoter in the present model mediated overexpression of VEGF in all tubular segments that resulted in multiple changes in the tubulo-interstitium as well as in glomeruli and to increased levels of VEGF in the serum. Because there is no intrarenal pathway for VEGF released in the tubulointerstitial compartment to gain access to the glomerular tuft, we interpreted the glomerular changes as the consequence of the elevated VEGF serum levels.

Tubulointerstitial Effects

The tubulointerstitial effects were interesting in several respects. First, the newly formed capillaries frequently

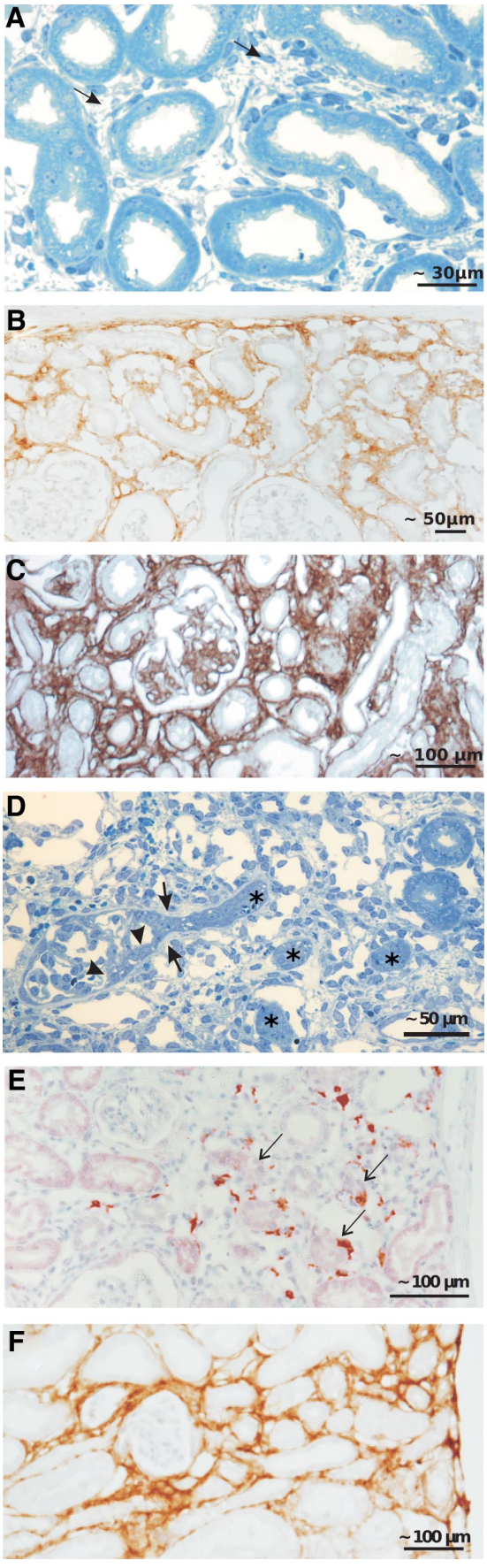

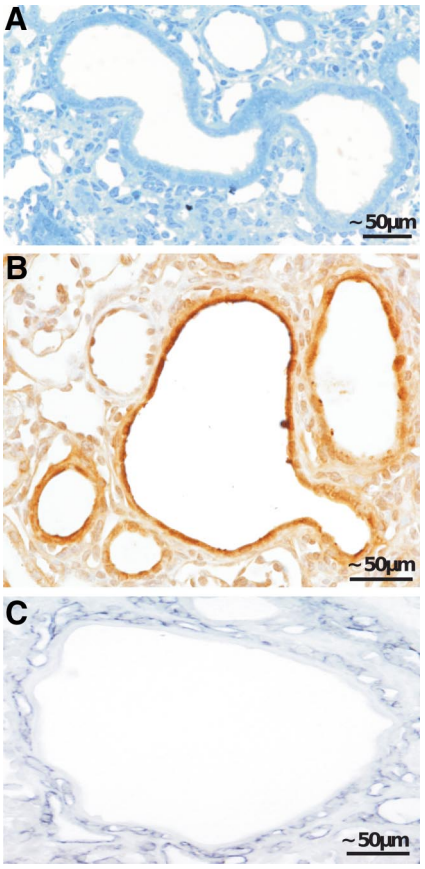

Figure 7. Cyst formation within renal tubules. **A–C:** Tubular cysts of a proximal tubule (**A**). **B** and **C:** Immunohistochemistry showing the strong staining against VEGF in the cystic epithelium (**B**) and the high density of capillaries surrounding the cyst (**C**; shown with an antibody against Meca 32).

contained portions of endothelium with pores without a diaphragm as is typically observed in glomerular capillaries instead of fenestrae with diaphragms as is observed in peritubular capillaries. This supports the notion that high doses of VEGF are necessary and sufficient to initiate pore formation in endothelial cells.[4]

Second, high local levels of VEGF seem to account for tubular cyst formation in this model as well. A role of VEGF in cyst development has recently been suggested.[7] Inhibition of VEGF receptors 1 and 2 in a rat model of polycystic kidney disease led to a decrease in cell proliferation and slowed the progression of cyst development. In the present model, the cystic tubules consistently showed high epithelial expression of VEGF, probably leading to a strong autocrine and paracrine

Figure 6. Changes within the interstitium. **A–C**: Development of fibrosis around intact tubules. Already after 2 weeks of DOX (**A**), more pronounced after 4 weeks (**C** and **D**), a dense fibrotic tissue (**arrows** in **A**) is encountered that contains collagen I (**B**) and collagen IV (**C**) as shown by immunohistochemistry. **D–F:** Focal interstitial fibrosis associated with the atrophy/degeneration of a nephron. **D:** Glomerular profile with tuft adhesion and proliferative process at Bowman's capsule (between two **arrowheads**), expansion of the parietal basement membrane (**arrows**), and encroachment on the tubule. The complete obstruction of the urinary orifice was verified by tracing in serial sections. Note the corresponding atrophic tubules (**asterisks**) in the vicinity surrounded by fibrous tissue. **E** and **F:** Immunohistochemistry showing the numerous macrophages (**E**; ER-HR3 staining) and the dense accumulation of collagen I in such areas (**F**). **Arrows** in **E** denote red-stained macrophages.

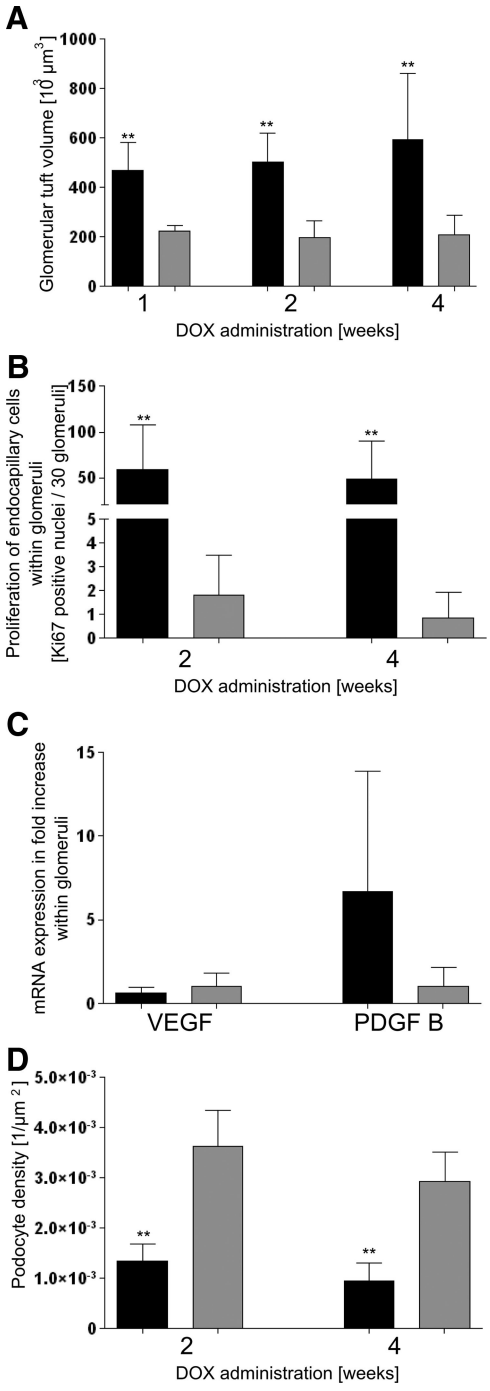

Figure 8. Values of experimental animals in black, controls in gray columns; shown are the means ± SD. **A:** Glomerular tuft volume; a dramatic increase is seen after 1, 2, and 4 weeks of DOX in transgenic animals. $N = 7$; $^{**}P < 0.01$. **B:** Proliferation of endocapillary cells within glomeruli. After 2 and 4 weeks of DOX, the number of Ki-67-positive endocapillary cells (including mesangial and endothelial cells) is drastically increased in transgenic mice. $N = 7$; $^{**}P < 0.01$. **C:** mRNA expression within glomeruli. After 4 weeks of DOX, VEGF within glomeruli of transgenic animals shows a tendency to decrease whereas PDGF-B increases. $N = 4$. **D:** Podocyte density. Transgenic animals show a dramatic decrease in podocyte density of glomeruli after 2 and 4 weeks of DOX. N(transgenics) = 7, N(controls) = 5; $^{**}P < 0.01$.

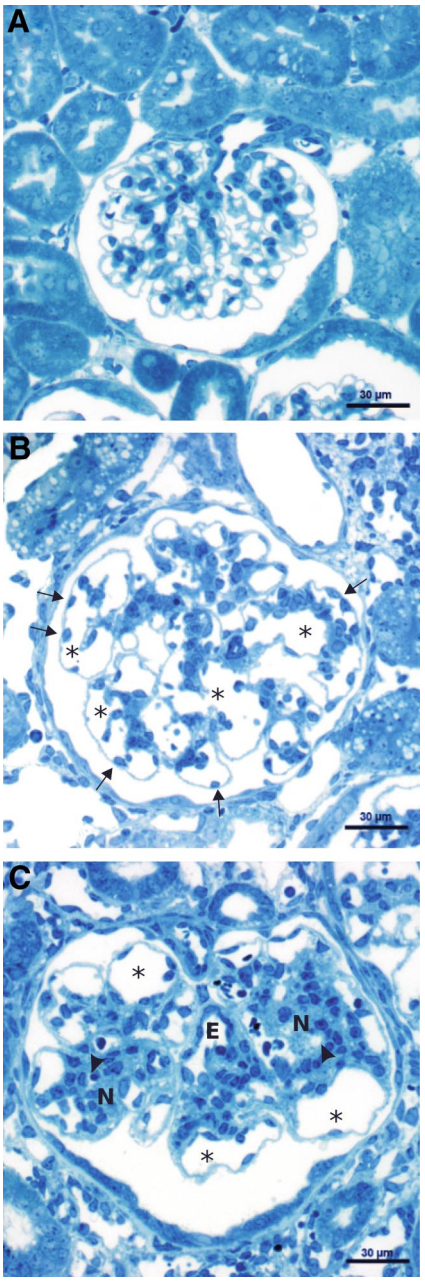

Figure 9. Glomerular changes. **A:** Control; note the numerous uniformly small capillary profiles. **B:** After 2 weeks of DOX, giant glomeruli with fewer but considerably lager capillary profiles (**asterisks**) are prominent. Frequently, endothelial cell bodies are lying at unusual peripheral positions (**arrows**). Note the islands of clustered mesangium. **C:** After 4 weeks of DOX, individual giant glomerular capillaries (**asterisks**) are still seen, otherwise mesangial nodules (N) developed that contain either small or completely collapsed capillaries (**arrowheads**). Note the intraglomerular segment of the efferent arteriole (E) that is densely equipped with endothelial cells (seen in both glomeruli).

stimulations. Cystic tubules always exhibited the most intensive VEGF staining.

Third, the role of VEGF in development of renal fibrosis has been the subject of some controversy.[6] In the present model, VEGF strongly stimulated the proliferation of fibroblasts. Moreover, the acquisition of α-SMA by 5′NT-positive interstitial cells (as shown previously)[21,22] suggests that VEGF induced the conversion of fibroblasts into myofibroblasts, leading to an exceptional high density of these cells. These effects were most probably mediated by TGF-β and PDGF-B produced by endothelial cells in response to VEGF; both cytokines are known

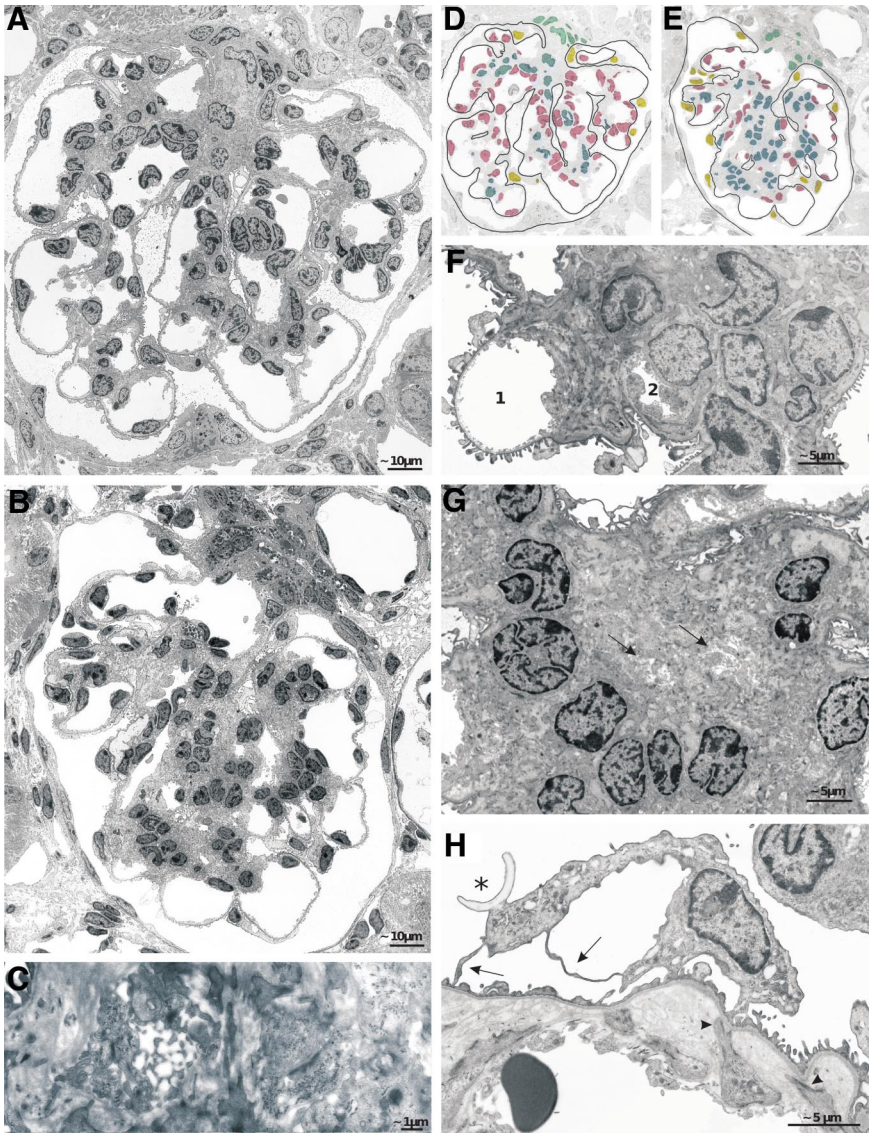

Figure 10. Glomerular changes; TEM details. **A**, **B**, **D**, and **E:** Glomerular profiles after 2 (**A** and **D**) and 4 weeks (**B** and **E**) of DOX treatment; **D** and **E** indicate the cellular composition in both profiles (nuclei of endothelial cells are shown in red, of mesangial cells in blue, of podocytes in yellow, and of extraglomerular mesangial cells in turquoise). After 2 weeks of DOX capillary enlargement and endothelial proliferation (red-labeled cells) and after 4 weeks mesangial proliferation (blue-labeled cells) are dominant. Note that the podocyte foot processes are generally well preserved. **C:** A capillary in the process of strangulation and collapse. **F:** A stage after 4 weeks of DOX showing the incorporation of capillaries (1 and 2) into an expanding mesangial nodule. Mesangial cells extend toward the periphery at both sides of 1 and the almost total embracement and collapse of 2; note that the podocyte foot processes of this capillary are partially effaced. **G:** A mesangial nodule consisting of cells and matrix that contains the collapsed remnants of at least two capillaries (**arrows**). **H:** An apparently hypoplastic podocyte with primary processes (**arrow**) that are extended into thin sheets. Note the partial foot process effacement and the shedding of a portion of an apical membrane (**asterisk**) into Bowman's space. Furthermore, the separation of the endothelium from the GBM by the expanding mesangium is seen; mesangial cell processes still fix to the GBM (**arrowheads**).

to induce this conversion.[23–25] Myofibroblasts are capable of matrix production[24] and are the most likely source of the large amounts of matrix in this model.

Thus, at early stages of the disease, a unique kind of fibrosis had developed characterized by abundance of fibroblasts/myofibroblasts and of collagenous fibers as well as capillaries but intact tubules. In later stages, areas of classic fibrosis associated with degenerating tubules appeared in a focal distribution secondary to glomerular degeneration (see below). Thus, two different types of fibrosis were seen side-by-side, with and without tubular decomposition. This supports the notion that fibrosis per se is not necessarily harmful to tubules and that the focal fibrosis found in many glomerular diseases is secondary to nephron degeneration, not the reverse.[26]

Glomerular Injury

In the first 2 weeks, all glomeruli displayed severe injuries that indicated a deranged cross-talk between podocytes and the endocapillary compartment, suggesting a significant susceptibility of the glomerular architecture to changes in VEGF signaling. At present, VEGF blockade has assumed an important new role in the treatment of cancer.[27,28] In a fraction of patients, the anti-VEGF therapy causes significant glomerular disease, mostly a kind of thrombotic microangiopathy.[29] Indeed, it has been experimentally proven that this glomerular disease derives from a decreased availability of VEGF within the glomerulus.[30]

So far, two publications[4,31] have reported glomerular changes in animal models of VEGF overexpression. In a mouse model, podocyte-specific overexpression of VEGF started already at birth and thus interfered with normal nephron development; this led to misshaped glomeruli of the collapsing type.[4] In rabbits,[31] overexpression of VEGF in liver and kidney glomeruli (probably including the podocytes) led to quite different results glomerular hypertrophy based on endothelial, and somewhat later, mesangial cell proliferation was also found in

this study.[31] Differences were seen in the response of podocytes that were hypertrophied and exhibited foot process effacement and leakiness to serum proteins in the rabbit model but were unchanged in size and generally had intact foot processes in our model. The different outcomes are probably a consequence of the extent of the increase in VEGF serum levels in our study.

In the present model, the increased VEGF serum levels appear to have initiated a feedback-mediated decrease in VEGF production by podocytes, and this combination of increased serum levels but decreased local production of VEGF may account for the particular form of glomerular injury. Normally, VEGF produced by podocytes is probably the only VEGF present in the glomerulus; it controls the development, maintenance, and repair of the glomerular tuft.[32,33] The proper effects largely depend on a correct dosage[4] and on an asymmetric intraglomerular distribution of VEGF. To reach the endocapillary compartment, VEGF secreted by podocytes has to spread by diffusion through the GBM toward the center of the tuft; thus, we expect a concentration profile with highest concentrations at the podocyte dissipating toward the center of a lobule. This gradient appears to be essential for the proper organization of glomerular lobules whereby capillaries are arranged at the periphery with their filtration surface abutting the urinary space and with the endothelial cell bodies bordering the mesangium.

In response to VEGF, as known from studies of glomerular development,[34,35] endothelial cells produce PDGF-B (and possibly other mediators) that stimulates mesangial cell proliferation and directs these cells toward the capillaries, where they adhere to the GBM in between capillaries. The centripetal pull on the GBM by mesangial cells together with a centrifugal growth of capillaries leads to the bulging of capillaries into the urinary space.[2]

In the present model, high levels of serum VEGF decreased VEGF production by podocytes and abolished any concentration gradient within the tuft and thus the stimulus for directed capillary growth. One sign of an undirected growth was the abnormal positioning of many endothelial cell bodies away from the mesangial compartment but close to podocytes. As a further consequence, PDGF (or any additional mediator produced by endothelial cells) became available at peripheral sites, attracting mesangial cells into the space between the GBM and the endothelium. Thereby, the glomerular lobules were transformed into random conglomerates of capillaries and mesangium that finally presented as mesangial nodules (schematically depicted in Supplemental Figure S5, see *http://ajp.amjpathol.org*), which are strikingly similar to early lesions in diabetic glomerulopathy generally designated as diffuse/nodular intercapillary sclerosis.[36]

Since in the present model transgenic production of VEGF lacks any feedback control, VEGF was continuously available within the glomerulus, accounting for ongoing stimulation. We suggest that capillaries and mesangial cells "competed" for the available space inside the GBM. In advanced stages, mesangial proliferation appears to dominate over capillary proliferation leading to compression and strangulation of capillaries. On the other hand, since mesangial proliferation depends, at least in part, on PDGF-B produced by endothelial cells, a kind of equilibrium probably developed between these cell types that accounted for the survival of the severely damaged glomeruli.

Secondary Changes

The degeneration of glomeruli and subsequently of the entire nephron was clearly initiated by another type of change that developed focally on top of the model-specific damage. As established in previous studies of degenerative and proliferative glomerular diseases,[16,37] this pathway started with the formation of tuft adhesions to Bowman's capsule and proceeded by enroachment of the capsular process onto the tubule via the urinary pole. Tracing in serial sections in the present study revealed the same mechanism, ie, degeneration of tubules eventually resulting in focal fibrosis only occurred in nephrons with obstructed urinary orifice. This fully agrees with the establishment of focal fibrosis in other relevant models.[26]

This present scenario of mixed changes—consisting of specific lesions, secondary lesions of the focal segmental glomerulosclerosis type and focal areas of tubular degeneration and fibrosis—has striking similarities with the pathology in human diabetic nephropathy. In diabetic retinopathy,[38–40] a crucial role of increased VEGF is firmly established, whereas the role of VEGF in diabetic nephropathy is a matter of controversy.[5,8,41–43] The diffuse/early nodular lesions seen in diabetic glomerulopathy consist of a disorganized mixture of capillaries and mesangium, enclosed by a bulged sack of GBM covered with fairly intact podocytes—like the specific changes in the present model. Note, a deranged balance between systemic and locally produced VEGF may also be rooted in a decreased availability of podocyte-derived VEGF in the endocapillary compartment. The progressing thickening of the GBM in diabetic glomerulopathy may well account for a progressing deficit. Further studies are needed whether the structural similarities are based on comparable mechanisms.

Acknowledgments

We thank Ingrid Hartmann und Ulrike Sonnek for technical assistance and Rolf Nonnenmacher for preparing the schematic drawings. Kevin Lemley contributed valuable critique.

References

1. Holmes DI, Zachary I: The vascular endothelial growth factor (VEGF) family: angiogenic factors in health and disease. Genome Biol 2005, 6:209
2. Kriz W: Ontogenetic development of the filtration barrier. Nephron Exp Nephrol 2007, 106:e44–e50
3. Eremina V, Quaggin SE: The role of VEGF-A in glomerular development and function. Curr Opin Nephrol Hypertens 2004, 13:9–15
4. Eremina V, Sood M, Haigh J, Nagy A, Lajoie G, Ferrara N, Gerber HP, Kikkawa Y, Miner JH, Quaggin SE: Glomerular-specific alterations of

VEGF-A expression lead to distinct congenital and acquired renal diseases. J Clin Invest 2003, 111:707–716
5. Schrijvers BF, Flyvbjerg A, De Vriese AS: The role of vascular endothelial growth factor (VEGF) in renal pathophysiology. Kidney Int 2004, 65:2003–2017
6. Kang DH, Johnson RJ: Vascular endothelial growth factor: a new player in the pathogenesis of renal fibrosis. Curr Opin Nephrol Hypertens 2003, 12:43–49
7. Tao Y, Kim J, Yin Y, Zafar I, Falk S, He Z, Faubel S, Schrier RW, Edelstein CL: VEGF receptor inhibition slows the progression of polycystic kidney disease. Kidney Int 2007, 72:1358–1366
8. Chen S, Ziyadeh FN: Vascular endothelial growth factor and diabetic nephropathy. Curr Diab Rep 2008, 8:470–476
9. Traykova-Brauch M, Schonig K, Greiner O, Miloud T, Jauch A, Bode M, Felsher DW, Glick AB, Kwiatkowski DJ, Bujard H, Horst J, von Knebel Doeberitz M, Niggli FK, Kriz W, Grone HJ, Koesters R: An efficient and versatile system for acute and chronic modulation of renal tubular function in transgenic mice. Nat Med 2008, 14:979–984
10. Akeson AL, Greenberg JM, Cameron JE, Thompson FY, Brooks SK, Wiginton D, Whitsett JA: Temporal and spatial regulation of VEGF-A controls vascular patterning in the embryonic lung. Dev Biol 2003, 264:443–455
11. Kaissling B, Kriz W: Variability of intercellular spaces between macula densa cells: a transmission electron microscopic study in rabbits and rats. Kidney Int Suppl 1982, 12:S9–S17
12. Richardson KC, Jarett L, Finke EH: Embedding in epoxy resins for ultrathin sectioning in electron microscopy. Stain Technol 1960, 35:313–323
13. Weibel ER: Stereological methods: practical methods for biological morphometry. London AP. London, 1979, pp 35–51
14. Theilig F, Bostanjoglo M, Pavenstadt H, Grupp C, Holland G, Slosarek I, Gressner AM, Russwurm M, Koesling D, Bachmann S: Cellular distribution and function of soluble guanylyl cyclase in rat kidney and liver. J Am Soc Nephrol 2001, 12:2209–2220
15. Gandhi R, Le Hir M, Kaissling B: Immunolocalization of ecto-5′-nucleotidase in the kidney by a monoclonal antibody. Histochemistry 1990, 95:165–174
16. Kriz W, Hahnel B, Hosser H, Ostendorf T, Gaertner S, Kranzlin B, Gretz N, Shimizu F, Floege J: Pathways to recovery and loss of nephrons in anti-Thy-1 nephritis. J Am Soc Nephrol 2003, 14: 1904–1926
17. Takemoto M, Asker N, Gerhardt H, Lundkvist A, Johansson BR, Saito Y, Betsholtz C: A new method for large scale isolation of kidney glomeruli from mice. Am J Pathol 2002, 161:799–805
18. Jugold M, Palmowski M, Huppert J, Woenne EC, Mueller MM, Semmler W, Kiessling F: Volumetric high-frequency Doppler ultrasound enables the assessment of early antiangiogenic therapy effects on tumor xenografts in nude mice. Eur Radiol 2008, 18:753–758
19. Strutz F, Zeisberg M: Renal fibroblasts and myofibroblasts in chronic kidney disease. J Am Soc Nephrol 2006, 17:2992–2998
20. Simon M, Grone HJ, Johren O, Kullmer J, Plate KH, Risau W, Fuchs E: Expression of vascular endothelial growth factor and its receptors in human renal ontogenesis and in adult kidney. Am J Physiol 1995, 268:F240–F250
21. Maxwell PH, Ferguson DJ, Nicholls LG, Johnson MH, Ratcliffe PJ: The interstitial response to renal injury: fibroblast-like cells show phenotypic changes and have reduced potential for erythropoietin gene expression. Kidney Int 1997, 52:715–724
22. Picard N, Baum O, Vogetseder A, Kaissling B, Le Hir M: Origin of renal myofibroblasts in the model of unilateral ureter obstruction in the rat. Histochem Cell Biol 2008, 130:141–155
23. Czochra P, Klopcic B, Meyer E, Herkel J, Garcia-Lazaro JF, Thieringer F, Schirmacher P, Biesterfeld S, Galle PR, Lohse AW, Kanzler S: Liver fibrosis induced by hepatic overexpression of PDGF-B in transgenic mice. J Hepatol 2006, 45:419–428
24. Hinz B: Formation and function of the myofibroblast during tissue repair. J Invest Dermatol 2007, 127:526–537
25. Floege J, Eitner F, Alpers CE: A new look at platelet-derived growth factor in renal disease. J Am Soc Nephrol 2008, 19:12–23
26. Kriz W, LeHir M: Pathways to nephron loss starting from glomerular diseases-insights from animal models. Kidney Int 2005, 67:404–419
27. Duda DG, Batchelor TT, Willett CG, Jain RK: VEGF-targeted cancer therapy strategies: current progress, hurdles and future prospects. Trends Mol Med 2007, 13:223–230
28. Zhu X, Wu S, Dahut WL, Parikh CR: Risks of proteinuria and hypertension with bevacizumab, an antibody against vascular endothelial growth factor: systematic review and meta-analysis. Am J Kidney Dis 2007, 49:186–193
29. Stokes MB, Erazo MC, D'Agati VD: Glomerular disease related to anti-VEGF therapy. Kidney Int 2008, 74:1487–1491
30. Eremina V, Jefferson JA, Kowalewska J, Hochster H, Haas M, Weisstuch J, Richardson C, Kopp JB, Kabir MG, Backx PH, Gerber HP, Ferrara N, Barisoni L, Alpers CE, Quaggin SE: VEGF inhibition and renal thrombotic microangiopathy. N Engl J Med 2008, 358:1129–1136
31. Liu E, Morimoto M, Kitajima S, Koike T, Yu Y, Shiiki H, Nagata M, Watanabe T, Fan J: Increased expression of vascular endothelial growth factor in kidney leads to progressive impairment of glomerular functions. J Am Soc Nephrol 2007, 18:2094–2104
32. Vaughan MR, Quaggin SE: How do mesangial and endothelial cells form the glomerular tuft? J Am Soc Nephrol 2008, 19:24–33
33. Shimizu A, Masuda Y, Mori T, Kitamura H, Ishizaki M, Sugisaki Y, Fukuda Y: Vascular endothelial growth factor165 resolves glomerular inflammation and accelerates glomerular capillary repair in rat anti-glomerular basement membrane glomerulonephritis. J Am Soc Nephrol 2004, 15:2655–2665
34. Lindahl P, Hellstrom M, Kalen M, Karlsson L, Pekny M, Pekna M, Soriano P, Betsholtz C: Paracrine PDGF-B/PDGF-Rβ signaling controls mesangial cell development in kidney glomeruli. Development 1998, 125:3313–3322
35. Betsholtz C, Lindblom P, Bjarnegard M, Enge M, Gerhardt H, Lindahl P: Role of platelet-derived growth factor in mesangium development and vasculopathies: lessons from platelet-derived growth factor and platelet-derived growth factor receptor mutations in mice. Curr Opin Nephrol Hypertens 2004, 13:45–52
36. Fioretto P, Mauer M: Histopathology of diabetic nephropathy. Semin Nephrol 2007, 27:195–207
37. Kriz W, Hosser H, Hahnel B, Gretz N, Provoost AP: From segmental glomerulosclerosis to total nephron degeneration and interstitial fibrosis: a histopathological study in rat models and human glomerulopathies. Nephrol Dial Transplant 1998, 13:2781–2798
38. Sydorova M, Lee MS: Vascular endothelial growth factor levels in vitreous and serum of patients with either proliferative diabetic retinopathy or proliferative vitreoretinopathy. Ophthalmic Res 2005, 37:188–190
39. Maier R, Weger M, Haller-Schober EM, El-Shabrawi Y, Wedrich A, Theisl A, Aigner R, Barth A, Haas A: Multiplex bead analysis of vitreous and serum concentrations of inflammatory and proangiogenic factors in diabetic patients. Mol Vis 2008, 14:637–643
40. Penn JS, Madan A, Caldwell RB, Bartoli M, Caldwell RW, Hartnett ME: Vascular endothelial growth factor in eye disease. Prog Retin Eye Res 2008, 27:331–371
41. Hovind P, Tarnow L, Oestergaard PB, Parving HH: Elevated vascular endothelial growth factor in type 1 diabetic patients with diabetic nephropathy. Kidney Int Suppl 2000, 75:S56–S61
42. Lindenmeyer MT, Kretzler M, Boucherot A, Berra S, Yasuda Y, Henger A, Eichinger F, Gaiser S, Schmid H, Rastaldi MP, Schrier RW, Schlondorff D, Cohen CD: Interstitial vascular rarefaction and reduced VEGF-A expression in human diabetic nephropathy. J Am Soc Nephrol 2007, 18:1765–1776
43. Lenz T, Haak T, Malek J, Grone HJ, Geiger H, Gossmann J: Vascular endothelial growth factor in diabetic nephropathy. Kidney Blood Press Res 2003, 26:338–343